# Rehabilitation of Cracked and Corroded Reinforced Concrete Beams with Fiber-Reinforced Plastic Patches

Chung-Yue Wang[1]; Chien-Chih Shih[2]; Shao-Chih Hong[3]; and Wei-Chih Hwang[4]

**Abstract:** The behavior under static loading of fiber-reinforced plastic (FRP) retrofitted reinforced concrete beams, possessing a high chloride content and rebar corrosion, was studied both experimentally and analytically. The test beams were characterized as falling into three different groups according to the state of their corrosion damage: (1) natural corrosion, (2) cathodic protection, and (3) accelerated corrosion. The load carrying capacities of the beams, with or without FRP patching, were tested in the laboratory. The experimental results show that the state of corrosion of the steel, the water/cement ratio of the concrete material, and the arrangement and the number of FRP patches all affect the strength as well as the failure mechanisms of retrofitted RC beams. Some simple analytical models and a design concept for retrofitting cracked and corroded RC beams with FRP sheets are also presented and discussed.

**DOI:** 10.1061/(ASCE)1090-0268(2004)8:3(219)

**CE Database subject headings:** Corrosion; Rehabilitation; Fiber reinforced polymers; Concrete, reinforced; Deterioration; Cracking; Beams; Cathodic protection; Composite materials.

## Introduction

The repair and rehabilitation of reinforced concrete structures in coasted areas is a major challenge to civil engineers. These structures often require repairs due to concrete deterioration caused by reinforcement corrosion, sulfate attack, salt weathering, or cracking due to environmental effects, and there is a potential for aggregate-cement reactivity to occur. These factors interact with each other to aggravate the deterioration processes (Dehwah et al. 1994). The existence of cracks and other damage is the main cause of structural fatigue and a reduction of the capability of the structure to sustain its design load. The corrosion of rebar can cause concrete cracking and spallation, consequently reducing the load carrying capacity and the safety of the structure. The purpose of repairs is to improve the function and performance of the structure, restore and increase the strength and stiffness of the concrete, improve the appearance of the concrete surface, increase water tightness, prevent access of corrosive materials to the reinforcing, and improve the overall durability of the structures.

Corrosion damage of ''sea sand houses'' and seaside bridges is believed to be caused by the high chloride content in the concrete and by poor concrete quality. The service life of corroded structures can be extended by strengthening and by corrosion protection. The proper repair of deteriorating concrete structures is based on the careful evaluation of the causes, extent, and consequences of the deterioration, and the repair techniques, procedures, and materials necessary to remedy the situation. The cost and ease of application, and the efficiency of the repair process are major considerations in choosing the materials and techniques.

Composite patches are lighter than steel plate and hence easier to handle. They have a high specific stiffness and weight/strength ratios, outstanding fatigue behavior, and are corrosion resistant. They can be easily bonded to the concrete surface on-site, without the use of extensive scaffolding and jacks, requiring minimum amount of support equipment. In addition, they can be formed on-site and hence can be used in very close quarters and in areas where access is limited. The lower total weight not only increases the ease of the retrofitting, but also is more cost-efficient (Karbhari and Engineer 1996). Although the composite patching technique has been investigated by a number of researchers (Jones et al. 1980; Ehsani and Saadatmanesh 1990; Sonobe et al. 1997; GangaRao and Vijay 1998; Nanni et al. 1998; Saadatmanesh and Malek 1998; Theriault and Benmokrane 1998), the overall effectiveness of using fiber-reinforced plastic (FRP) to retrofit corroded, cracked reinforced concrete (RC) beams has not been well investigated.

This paper evaluates the effectiveness of combining the corrosion protection and the FRP strengthening techniques. Some analytical models are developed to estimate the ultimate load carrying capacity of corroded FRP patched RC beams. We emphasize the structural mechanical aspects, rather than the corrosion mechanism aspects.

## Experimental Program

To study the behavior of reinforced concrete, beams with rebar corrosion and a high chloride content under static loading test beams were first characterized, forming three different groups according to corrosion damage: (1) natural corrosion, (2) cathodic protection, and (3) accelerated corrosion. Two types of concrete

[1]Professor, Dept. of Civil Engineering, National Central Univ., Chungli, Taiwan 32054, R.O.C.

[2]Senior Engineer and Manager, Material Research Laboratory, Industrial Technology Research Institute, Hsinchu, Taiwan 310, R.O.C.

[3]Graduate Student, Dept. of Civil Engineering, National Central Univ., Chungli, Taiwan 32054, R.O.C.

[4]Graduate Student, Dept. of Civil Engineering, National Central Univ., Chungli, Taiwan 32054, R.O.C.

Note. Discussion open until November 1, 2004. Separate discussions must be submitted for individual papers. To extend the closing date by one month, a written request must be filed with the ASCE Managing Editor. The manuscript for this paper was submitted for review and possible publication on January 14, 2000; approved on October 21, 2002. This paper is part of the ***Journal of Composites for Construction***, Vol. 8, No. 3, June 1, 2004. ©ASCE, ISSN 1090-0268/2004/3-219–228/$18.00.

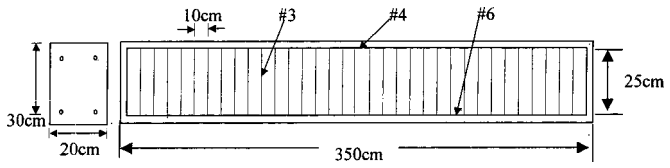


**Fig. 1.** Details of reinforcement in beam specimen

were used in each group. The first type, noted by the letter H in this study, has a compression strength of about 222.5 kg/cm$^2$. The other type, noted by the letter L, has a compression strength around 75 kg/cm$^2$. This low strength concrete material was selected to simulate the poor quality concrete typically found in some civilian structures in Taiwan. The concrete materials were mixed with salt in order to increase the chloride content of the specimens and to improve conductivity of the resultant concrete, so that accelerated galvanic corrosion could be induced by an external current supply.

### *Casting of Reinforced Concrete Beams*

Twenty-four 20×35×350 cm reinforced concrete beams were cast and divided into two groups, denoted by L and H according to the compression strength of their concrete. In group H, there were nine beams cast from concrete with a compression strength ($f'_c$) equal to 222.5 kg/m$^2$. The water/cement ratio was 0.71 and the chloride content 7.2 kg/m$^3$. Two number 6 steel bars of diameter 19.1 mm were used as the bottom bars, and two number 4 bars of diameter 9.53 mm were used as the top bars. Stirrups of number 3 bars of diameter 19.1 mm were spaced every 10 cm along the length of the beams. The yielding stress of the reinforcement was around 3,760 kg/cm$^2$ and the elastic modulus was

**Table 1.** Coding System of Test Beams

| Code | Beam | Description |
|---|---|---|
| I | H | Compression strength of concrete = 222.5 kg/cm$^2$ |
| | L | Compression strength of concrete = 75 kg/cm$^2$ |
| II | A1 | Low input of accelerated corrosion power |
| | A2 | High input of accelerated corrosion power |
| | P1 | Cathodic protection (with one 10 cm wide longitudinal FRP strip) |
| | P2 | Cathodic protection (with two 5 cm wide longitudinal FRP strips) |
| | N | Naturally corroded under room environment |
| | O | No chloride content in the specimen |
| III | T0 | No longitudinal FRP strip on tension side |
| | T1 | One layer of 10 cm wide longitudinal FRP strip on tension side |
| | T2 | Two layers of 10 cm wide longitudinal FRP strip on tension side |
| | E | Cracks sealed by epoxy injection |
| | U2 | 10 cm wide U-shaped anchorage at the ends of longitudinal FRP strip |
| | U10 | U-shaped FRP strips of width 10 cm at a spacing of 20 cm along the beam |
| | D10 | All U-shaped FRP strips of width 10 cm at a spacing of 20 cm along the beam axis were cut at both corners of the beam's tensile side |

Note: I (concrete strength), II (corrosion state), and III (FRP patching style).

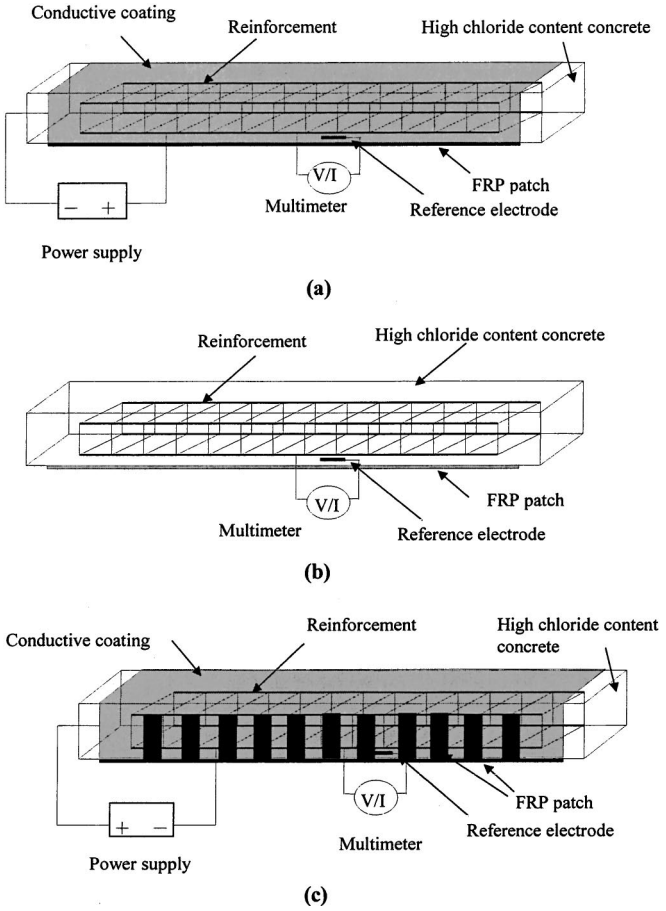


**Fig. 2.** Schematic representation of test setups for measuring corrosion rates of steel bars for different groups: (a) accelerated corrosion; (b) natural corrosion; and (c) corrosion protected

equal to 2.04×10$^6$ kg/cm$^2$. Fig. 1 shows details of the reinforcement used in the beams. In group L, there were 15 beams cast from concrete with a compression strength ($f'_c$) equal to 75 kg/cm$^2$, a water/cement ratio of 0.9, and a chloride content of 7.2 kg/m$^3$. Due to the high water/cement ratio of the low compressive strength beams, most of the coarse aggregates sank to the bottom. This in-homogeneity caused the strength of the concrete material within the upper zone to be lower. Therefore, to prevent the compression failure of the tested beam, all the beams in this group were inverted and the side with the higher compression strength (75 kg/cm$^2$) used as the beam compression side. Hence, in this group, the top reinforcements, two number 6 bars and two number 4 bars, became the bottom reinforcements.

To more easily analyze the character of the test beams, all the specimens were coded according to their concrete strength, corrosion state, and FRP patching style. The definitions of all the code letters are listed in Table 1. It is noted that T1U10 means that the patching sequence is T1 first, then U10. U10T1 means the T1 was patched after and outside of U10. After casting, the specimens were cured and naturally corroded for periods ranging between 9,336 and 11,376 h, as shown in Tables 2 and 3.

### *Corrosion Monitoring*

Fig. 2 shows the associated test setup for monitoring and measuring the corrosion rate of specimens in the different test groups. Since the objective of this research is to evaluate the effectiveness

**Table 2.** Total Corrosion Power of Induction Current for Reinforced Concrete Beams With Compression Strength of 222.5 kg/cm$^2$

| Beam | H-A2-T0 | | H-A2-ET1U10 | | | H-A1-T0 | | | H-A1-ET1U10 | | |
|---|---|---|---|---|---|---|---|---|---|---|---|
| Position | Left | Center | Left | Center | Right | Left | Center | Right | Left | Center | Right |
| Accelerated corrosion | | | | | | | | | | | |
| Power through conductive coating (A h) | | 361.9 | | 380 | | 464 | | | | 370 | |
| Power through titanium mesh (A h) | | 408 | | 408 | | 0 | | | | 0 | |
| Natural corrosion | | | | | | | | | | | |
| Elapsed period (h) | | 9,336 | | ,336 | | 9,816 | | | | 9,816 | |
| Corrosion rate ($\mu$A/cm$^2$) | 46 | 75 | 42–91 | 97 | 20–83 | 17–91 | 5–23 | 12–24 | 8–24 | 5–30 | 20 |
| Power through natural corrosion (A h) | 5,098 | 8,311 | 1,008–2,184 | 10,750 | 2,215–9,197 | 1,980–10,085 | 583–2681 | 1,399–2,796 | 931–2,796 | 641–3,494 | 2,330 |
| Total corrosion power (A h) | 5,868 | 9,081 | 1,796–2,972 | 11,538 | 3,003–9,985 | 2,444–10,549 | 1,047–3,145 | 1,863–3,260 | 1,301–3,166 | 1,011–3,864 | 2,700 |

of applying FRP tow-sheets to retrofit corroded reinforced concrete beams, the RC beam samples were first corroded. For the accelerated corrosion group, the surface of each beam was coated with a conductive material through which an electric current circulated to accelerate the corrosion process. However, it was found that the coated material became brittle and easily peeled off when subjected to a high electrical current after a certain period. In order to maintain a higher electrical current within these specimens, the A2 beams were also partially immersed in fiberglass tanks containing a sodium-chloride solution respectively connected by titanium mesh to the cathode and by rebar to the anode of the DC power supply. The corrosion activity in all the test beams was monitored by measuring the corrosion potential and the corrosion rate through some electrochemical techniques. Tables 2 and 3 show the total power applied to specimens with high and low compression strengths, in accelerated and natural corrosion environments, respectively. In these tables, natural corrosion power is denoted as NCP, as calculated by the following equation:

$$\text{NCP} = R \cdot t \cdot S \tag{1}$$

where $R$ = corrosion rate; $t$ = time elapsed in hours after casting; and $S$ = total surface area of the reinforcement material within a specimen. The total surface area of the reinforcement in each specimen is equal to 11,870 cm$^2$. To calculate the total surface area, only the vertical sides of each stirrup were accounted for, assuming that these parts were activated by the corrosion current.

The total volume deduction, $\Delta V$, due to the corrosion of the whole RC beam, can be estimated by the following equation. Eq. (2) is based on Faraday's law and the assumption that the corrosion state is uniformly distributed within the reinforcement material

$$\Delta V = \frac{I \cdot t \cdot M}{n \cdot F \cdot \rho} \tag{2}$$

where $F$ = Faraday's constant (96,500 A s); $I$ = current applied to the specimen; $M$ = atomic weight [$M$ (steel) = 56]; $\rho$ = density of the material (7.8 g/cm$^3$ for steel); and $n$ = valence of the reacting electrode (iron) for the material ($n_{\text{steel}} = 2$). $I \cdot t$ = total corrosion power (TCP) supplied to the RC beam and is in units of A s. The volume of each type of rebar deduced the total corrosion volume ($\Delta V$) is shared according to its surface area ($A_i$) within the RC beam. For example, the corrosion volume deduction of number 6 rebar, within the beam containing number 6, number 4, and number 3 types of rebar, is equal to

$$\Delta V_6 = \frac{A_6}{A_6 + A_4 + A_3} \cdot \Delta V \tag{3}$$

Based on the corrosion volume deduction value obtained from Eq. (3), the diameter size, $D_i^C$, of each type of corroded rebar could be calculated by the following equation:

**Table 3.** Total Corrosion Power of Induction Current for Reinforced Concrete Beams with Compression Strength of 75 kg/cm$^2$

| Beam | L-A2-T0 | L-A2-T2U2 | L-A2-T2D10 | L-A1-T0 | L-A1-T2U2 | | L-A2-T2D10 | |
|---|---|---|---|---|---|---|---|---|
| Position | Center | Center | Center | Center | Center | Right | Center | Right |
| Accelerated corrosion | | | | | | | | |
| Power through conductive coating (A h) | 409.2 | 408.2 | 399.6 | 433 | 438 | 438 | 410 | 410 |
| Power through titanium mesh (A h) | 1,122 | 1,122 | 1,122 | 0 | 0 | 0 | 0 | 0 |
| Natural corrosion | | | | | | | | |
| Elapsed period (h) | 10,056 | 10,056 | 10,056 | 11,376 | 11,376 | 11,376 | 11,376 | 11,376 |
| Corrosion rate ($\mu$A/cm$^2$) | 14 | 13 | 10 | 5 | 1.4 | 5–35 | 1.9–7.5 | 0.6–2 |
| Power through natural corrosion (A h) | 1,670 | 1,553 | 1,193 | 674 | 190 | 674–4,726 | 641 | 173 |
| Total corrosion power (A h) | 3,201 | 3,083 | 2,715 | 1,107 | 628 | 1,112–5,164 | 1,051 | 583 |

**Table 4.** Cross-Sectional Reduction of Rebar for Reinforced Concrete Beams with $f'_c = 222.5$ kg/cm$^2$

| Beam | H-A2-T0 | | H-A2-ET1U10 | | | H-A1-T0 | | | H-A1-ET1U10 | | |
|---|---|---|---|---|---|---|---|---|---|---|---|
| Position | Left | Center | Left | Center | Right | Left | Center | Right | Left | Center | Right |
| Total corrosion power (A h) | 5,868 | 9,081 | 1,296–2,792 | 11,538 | 3,003–9,985 | 2,444–10,549 | 1,047–3,145 | 1,863–3,260 | 1,301–3,166 | 1,011–3,864 | 2,700 |
| Diameter reduction of number 6 (mm) | 1.37 | 2.2 | 0.4–0.7 | 2.8 | 0.7–2.4 | 0.6–2.6 | 0.2–0.7 | 0.4–0.7 | 0.3–0.7 | 0.2–0.9 | 0.6 |
| Diameter reduction of number 4 (mm) | 1.4 | 2.2 | 0.4–0.7 | 2.9 | 0.7–2.5 | 0.6–2.7 | 0.2–0.7 | 0.4–0.7 | 0.3–0.7 | 0.2–0.9 | 0.6 |
| Diameter reduction of number 3 (mm) | 1.4 | 2.3 | 0.4–0.7 | 3.1 | 0.7–2.6 | 0.6–2.8 | 0.2–0.7 | 0.4–0.8 | 0.3–0.7 | 0.2–0.9 | 0.6 |

$$D_i^C = \sqrt{(D_i^0)^2 - \frac{\Delta V_i \cdot 4}{\pi \cdot N_i \cdot L_i}}, \quad (4)$$

where $D_i^0$ = original diameter of the number $i$ type rebar before corrosion testing; $L_i$ = length of each rebar unit (in the present study the unit length of each number 6 and number 4 rebar section is equal to 340 cm, while the unit length of the number 3 stirrup is $2 \times 25$ cm). $N_i$ = total number of number $i$ type rebar units ($N_6 = 2$, $N_4 = 2$, $N_3 = 34$ in the present study).

The cross-sectional diameter of each type of rebar after corrosion was calculated using Eq. (4) and the results are listed in Tables 4 and 5. These values will be used later in the analytical model to predict the response of all the tested beams. We used a corrosion rate of 5 $\mu$A/cm$^2$, which is a typical value measured in the field, to estimate the corresponding natural corrosion period of the beams. For example, the time after corrosion initiation for specimen H-A2-T0, calculated by Eq. (1), was approximately 11.1 years.

### *Repair Methods and Procedures*

Externally bonded FRP patches were formed on each of the corrosion-damaged beams using the wet-lay-up procedure suggested by the manufacturer. The composite HT1A-W12K, manufactured by the Industrial Technology Research Institute (ITRI) of Taiwan, was used. It is in the form of unidirectional tow sheets. Its properties are listed in Table 6. During the process, the dry fibrous reinforcement material, which is unidirectional in this case, is impregnated with resin during the actual placement. The composite is formed as it bonds to the concrete by a two-part resin system. The resin system thus serves the dual purpose of impregnating and bonding the fibers, as well as bonding the composite to the concrete. All the corroded specimens with cracks more than 0.2 mm wide were sealed by first injecting an epoxy before being patched with FRP strips.

The various arrangements of FRP patches are shown in Fig. 3. Seventeen RC beams were retrofitted using 10 cm wide FRP tow sheets on the tensile side of the beam, then patched by U-shaped FRP strips 10 cm wide spaced every 20 cm along the sides of the beams. The main reason for using the U-shaped strip was to prevent flexural or shear failure in the RC beam due to corrosion of the tensile reinforcement material. Besides, the U-shaped strips could be integrated with the beam, preventing separation from the concrete along longitudinal cracks due to corrosion. Beams belonging to the corrosion protection group were coated between the U anchorage strips with conductive material in which an electrical current was circulated. Although it is well known that continuous side patches along a beam's axis can greatly increase its loading capacity, the discontinuously distributed U-shaped FRP strips were required to provide the space with which to coat the conductive material for corrosion protection. This design also increases the shear capacity of the RC beams, and provides some compressive loading normal to the surface of the longitudinal FRP patch, preventing a premature debonding failure.

## Results and Discussion

### *Failure Modes of Test Beams*

The testing identified the following major failure modes:

Failure mode 1: The tensile steel yields and concrete compression crushing occurs.

Failure mode 2: The tensile steel yields and longitudinal FRP strips breaking occurs.

Failure mode 3: Longitudinal FRP strips debond first and then U anchorage strips near beam supports are torn down.

Failure mode 4: Longitudinal FRP strips debond.

Failure mode 5: Concrete beam undergoes compressive crushing but the compression steel does not yield.

A summary of the experimental results and the corresponding code number of failure modes are presented in Table 7. Fig. 4 shows the failure modes and the cracking patterns of some of the RC specimens tested.

In the experiments, failure mode (2), as shown in Fig. 4(b), was originally unexpected. Fig. 5 shows the strain variations during the loading process at points around the intersection of the

**Table 5.** Cross-Sectional Reduction of Rebar for RC Beams with $f'_c = 75$ kg/cm$^2$

| Beam | L-A2-T0 | L-A2-T2U2 | L-A2-T2D10 | L-A1-T0 | L-A1-T2U2 | | L-A1-T2D10 | |
|---|---|---|---|---|---|---|---|---|
| Position | Center | Center | Center | Center | Center | Right | Center | Right |
| Total corrosion power (A h) | 3,201 | 3,083 | 2,715 | 1,107 | 628 | 1,112–5,164 | 1,051 | 583 |
| Diameter reduction of number 6 (mm) | 0.7 | 0.7 | 0.6 | 0.3 | 0.1 | 0.3–12 | 0.2 | 0.1 |
| Diameter reduction of number 4 (mm) | 0.7 | 0.7 | 0.6 | 0.3 | 0.1 | 0.3–1.2 | 0.2 | 0.1 |
| Diameter reduction of number 3 (mm) | 0.7 | 0.7 | 0.6 | 0.3 | 0.1 | 0.3–1.2 | 0.2 | 0.1 |

**Table 6.** Basic Properties of Fiber Reinforcement Material, HT1A-W12K

| Fiber type | Weight ($g/cm^2$) | Tensile strength ($kg/cm^2$) | Tensile modulus ($kg/cm^2$) | Thickness (mm) | Ultimate strain (%) |
|---|---|---|---|---|---|
| Carbon | 200 | 7,868.5 | 507,970 | 0.502 | 1.55 |

U-shaped strip with the longitudinal FRP strip. In this figure, three strain values were measured along the direction of the fiber of the FRP material. One gauge on the U strip was used to measure the strain transverse to the fiber direction. The effects of the concentration of local strain, at the intersection of the U strip and the longitudinal strip, may have caused the FRP strip to break as this strain reached its ultimate value of 0.0155. In Fig. 5, it can be seen that the strain, str_fuc, in the direction of the U anchoring fiber, was close to zero during the loading process, and was under tension before the breakage of the longitudinal FRP fiber. The hoop stress that formed in the U strip during the later stages of its loading history had some effect on the breakage of the longitudinal strip fiber. The strain value of the longitudinal FRP at gauge "str_fb" crossing the U anchorage strip was almost half of the strain gauge value str_fm within the breakage zone after the yielding of the tensile steels, when the applied load reached 37 kN. Fig. 5 shows that the strain jumped at 37 kN. This represented a stress redistribution between the FRP strip and the RC beam due to the yielding of tensile steels and a local debonding failure at the FRP/concrete interface. To confirm and reduce the effects of stress concentration, we cut each U anchorage at the corners of the concrete beam [see Fig. 3(c)]. The strain distribution and intensity along the FRP strip are varied, as shown in Fig. 6. Comparing the strain value of the gauge "str_fm" in Fig. 6 with the strain gauge value at the same position in Fig. 5, one finds the strain concentration to be much reduced for the beam with discontinuous U anchorage strips, especially at load levels over 37 kN. The response curves of strain gauge "str_fb" in Fig. 5 and strain gauge "str_flm" in Fig. 6 are quite similar under various load levels. A detailed analysis of the local strain response due to the introduction of the U-shaped strip is not currently available. According to a previous analysis, done by Wang and Ling (1998), the occurrence of a local interfacial debonding failure between the FRP strip and the concrete beam is the main factor that causes the nonlinear behavior of the beam.

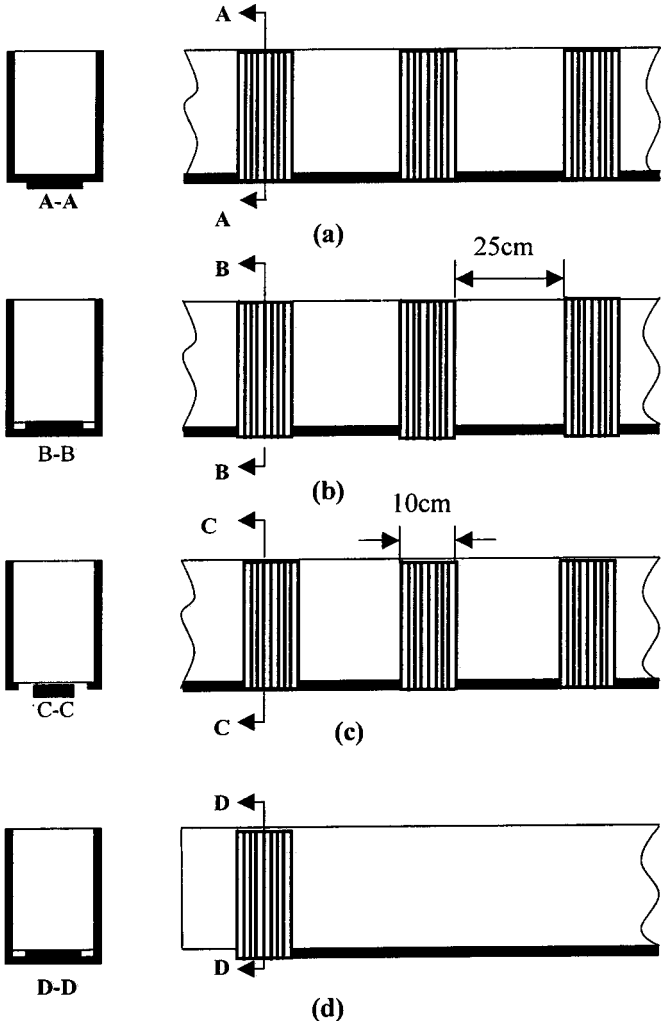


**Fig. 3.** Various fiber-reinforced plastic repairing schemes for corrosion damaged beams: (a) longitudinal strips patch over U anchorage strips; (b) longitudinal strip is wrapped in U anchorage strips; (c) longitudinal strip is wrapped in discontinuous U strips; and (d) U anchorage strips are applied only at the ends of the longitudinal strips

All beams without continuous U anchorage strips, such as L-A2-T2D10, L-A1-T2D10, L-N-T1D10, and L-N-T2, show FRP debonding failure. This type of failure is due mainly to the high interfacial shear stress between the FRP patch and the concrete beam, which formed after the yielding of the tensile steels during the loading process (Wang and Ling 1998). Failure mode (2), characterized by fiber breakage, shows that the arrangement of the U anchoring strips can increase the load carrying ratio of the FRP material locally, and then use its material's strength until breaking. It is believed that the ultimate load carrying capacity of the beam can be effectively increased if the stress concentration effect at the intersection area of U anchorages and longitudinal FRP strips can be improved.

### *Effects of Corrosion on Ultimate Load Carrying Capacity of Reinforced Concrete Beams*

It is well known that the load carrying capacity of RC beams decreases as the degree of corrosion damage to the reinforcement material increases. Fig. 7 shows the load-deflection curve of RC beams with different states of corrosion damage. Both the rigidity and the ultimate load capacity were reduced as the degree of corrosion damage was increased. In real cases, however, corrosion conditions are not uniformly distributed along a RC beam, and local pitting due to the corrosion is in-homogeneous which leads to different behaviors. In Fig. 8, two beams with the same retrofitting arrangement yielded first at points "a" and "f" of the load-deflection curves, respectively; then the longitudinal FRP strips partially debonded at points "b" and "f." They completely debonded at points "c" and "g." After this, the two U anchoring strips near the supports still held the longitudinal strips, and the longitudinal strips still provided some load carrying capacity due to the lifting force provided by stretching of the FRP strips along the bent surface. Once the U anchorage strip of beam L-A2-T2U2 broke at point "h," the load-deflection response was the same as the response curve of a corrosively damaged RC beam without FRP strengthening. However, the load-deflection curve of beam L-A1-T2U2 dropped suddenly at point "e" after the breaking of the steel due to the effects of corrosion pitting, which forms more easily in low strength concrete. This pitting phenomenon was

**Table 7.** Failure Modes and Ultimate Strengths of Fiber-Reinforced Plastic Retrofitted Reinforced Concrete Beams

| | Experimental results | | | Analytical predictions | | | |
|---|---|---|---|---|---|---|---|
| | | | | Saadatmanesh and Malek's model (1998) | | Moment-curvature method (Wang and Ling 1998) | |
| Specimen | Failure mode | Yielding load (kN) | Ultimate load (kN) | Ultimate load (kN)[a] | Failure mode | Ultimate load (kN)[a] | Failure mode |
| H-A2-T0 | 1 | 88.9 | 98.75 | 85.4 | 1 | 85.7 | 1 |
| H-A2-ET1U10 | 2 | 98.6 | 105.52 | 99.8 | 5 | 99.8 | 5 |
| H-A1-T0 | 1 | 90.8 | 100.58 | 91.5 | 1 | 91.9 | 1 |
| H-A1-ET1U10 | 2 | 105 | 106.23 | 106.8 | 5 | 107 | 5 |
| H-P1-T1U10 (a) | 2 | 106.1 | 114.53 | 110.4 | 5 | 110 | 5 |
| H-P1-T1U10 (b) | 2 | 100.7 | 104.6 | 110.4 | 5 | 110 | 5 |
| H-P2-T1U10 | 2 | 99 | 108.4 | 110.4 | 5 | 110 | 5 |
| H-O-T0 | 1 | 103.0 | 108 | 94.7 | 1 | 95.2 | 1 |
| H-O-T1U10 | 2 | 109.3 | 118 | 110.4 | 5 | 110 | 5 |
| L-A2-T0 | 1 | 42 | 43.95 | 38 | 1 | 38.1 | 1 |
| L-A2-T2U2 | 3 | 49.6 | 49.6 | 69.5 | 5 | 69.2 | 5 |
| L-A2-T2D10 | 4 | 42.6 | 47.73 | 69.5 | 5 | **49.39** | **4** |
| L-A1-T0 | 1 | 42.2 | 45.87 | 39.4 | 1 | 39.5 | 1 |
| L-A1-T2U2 | 3 | 53.8 | 53.85 | 70.5 | 5 | 70.8 | 5 |
| L-A1-T2D10 | 4 | 48.8 | 52.38 | 70.5 | 5 | **54.78** | **4** |
| L-P2-T1U10 (a) | 2 | 47.1 | 49.53 | 57.5 | 5 | 57.42 | 5 |
| L-P2-T1U10 (b) | 2 | 45.1 | 46.3 | 57.5 | 5 | 57.42 | 5 |
| L-P1-T1U10 (a) | 2 | 45.3 | 50.1 | 57.5 | 5 | 57.42 | 5 |
| L-P1-T1U10 (b) | 2 | 45.4 | 53 | 57.5 | 5 | 57.42 | 5 |
| L-N-T1U10 | 2 | 50.4 | 59.35 | 57.5 | 5 | 57.42 | 5 |
| L-N-T1D10 | 4 | 48.8 | 58.6 | 57.5 | 5 | **49.85** | **4** |
| L-N-U10T1 | 2 | 51.7 | 53.1 | 57.5 | 5 | 57.42 | 5 |
| L-N-T0 | 1 | 41.4 | 47.13 | 40.2 | 1 | 40.24 | 1 |
| L-N-T2 | 4 | 55.5 | 62.51 | 71.4 | 5 | **57.83** | **4** |

[a]Reduction of rebar diameters due to corrosion effects has been considered.

verified by removing the concrete material from the beam after the testing. The corrosion state of reinforcement materials of beam L-A2-T2U2 by removing part of its concrete is shown in Fig. 9.

### *Ultimate Loading Carry Capacity Affected by Arrangement of Fiber-Reinforced Plastic Strips*

Fig. 10 shows the load-deflection responses of no corrosion, low compression strength concrete beams with various types of FRP strip arrangements. In this figure, beam L-N-U10T1 yielded at point ''a.'' Its longitudinal FRP strip broke at point ''b.'' The longitudinal FRP strip of beam L-N-T1D10 debonded, and a crack propagated from the center toward the support at point ''c,'' in Fig. 10. The longitudinal FRP strip on beam L-N-T1U10 broke at point ''f'' and the concrete on the compression side was crushed at point ''g.'' The ultimate load of beam L-N-U10T1 was lower than that for beam L-N-T1U10, with the same amount of FRP material but placed in a different patching sequence. This was due to a premature debonding failure caused by a slope variation of the longitudinal FRP strip at the point where it intersected the U strip. Debonding is more easily formed at this intersection area especially when the longitudinal strips are under high tensile stress state. Fig. 10 also indicates that the ultimate strength, stiffness, ductility, and failure mode of RC beams, with the same amount of FRP material applied, will be affected by the arrangement and patching sequence of the FRP strips.

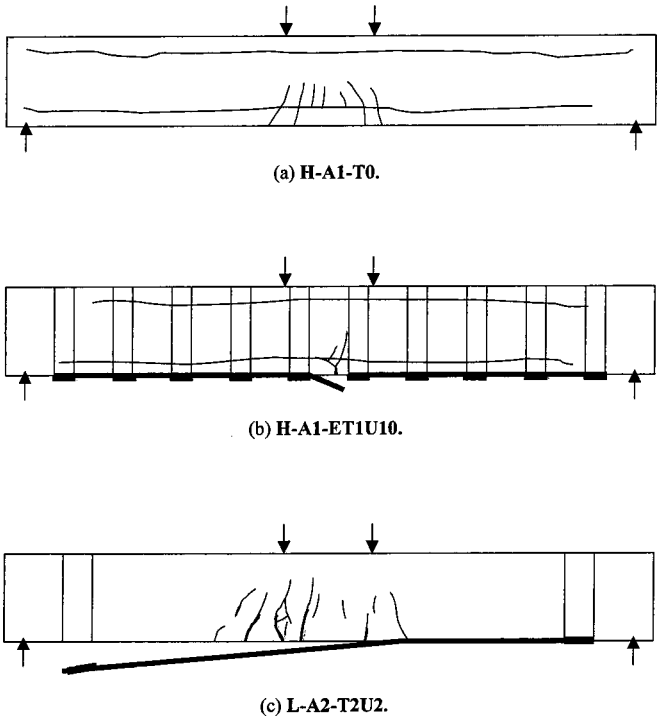


**Fig. 4.** Failure mode of specimen: (a) H-A1-T0; (b) H-A1-ET1U10; (c) L-A2-T2U2; (d) L-A2-T2D10; (e) L-N-T2; and (f) H-P2-T1U10

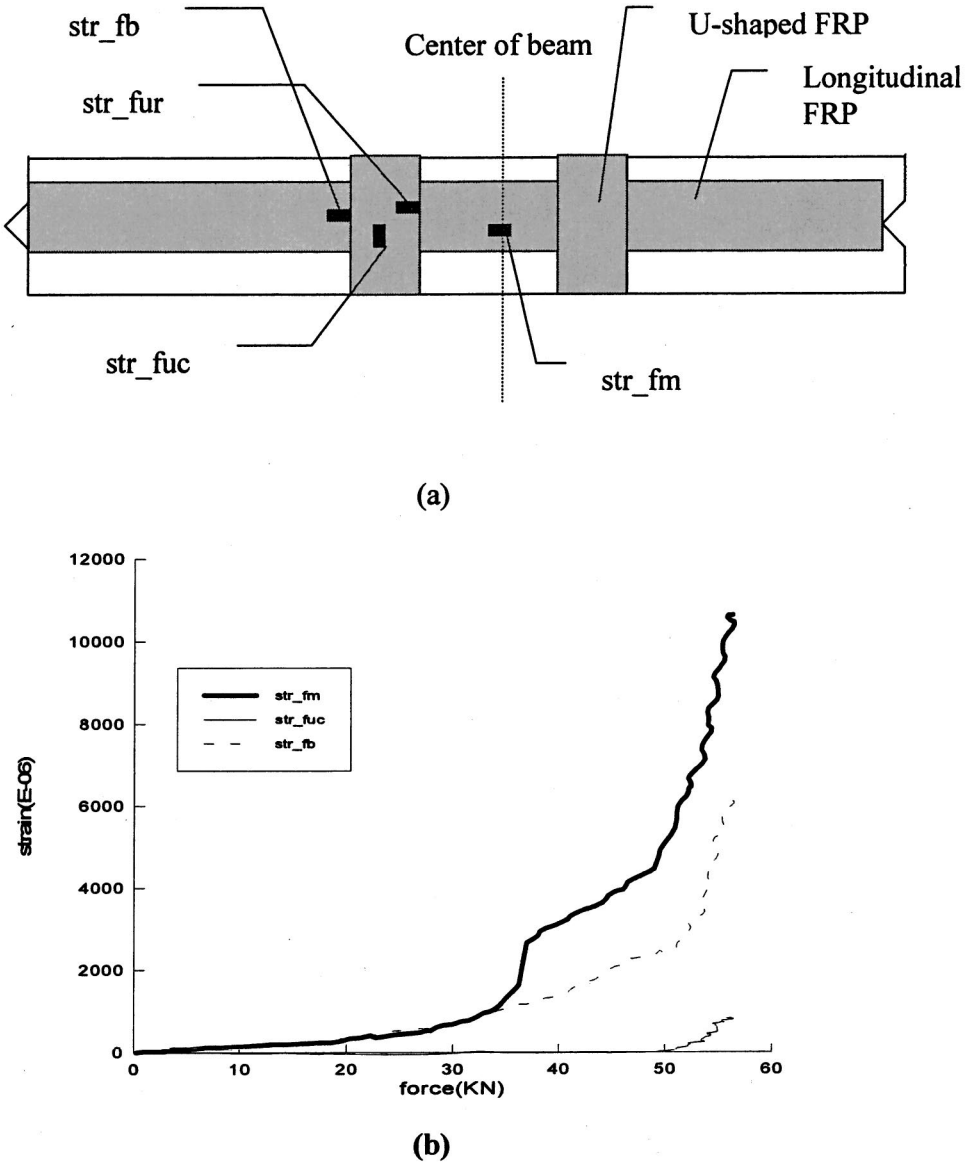


**Fig. 5.** Strain variations at some intersection points around the U anchorage with longitudinal fiber-reinforced plastic strips on beam L-N-T1U10: (a) arrangement of strain gauges on the tensile side of the beam; and (b) strain data at various load levels

### *Effectiveness of Cathodic Protection on Loading Carry Capacity of Reinforced Concrete Beams*

For the concrete that has salts in its constituents enough to cause corrosion, the corrosion is supposed to proceed and continue even after applying the sheets resulting in spalling of concrete and exerting pressure on FRP sheets. In this case, the applying of cathodic protection techniques on the FRP patched beams can decelerate the corrosion rate during their remaining service life. All the RC beams with high chloride content were corrosion protected 140 days after they were cast and different corrosion states had been formed already. Fig. 11 shows the load-deflection curves of the RC beams under cathodic protection. The yielding and failure mechanisms are similar to the ones without protection but using the same type of FRP retrofit. By checking the corrosion potential difference after 4 h power termination, it was found that both the corrosion potential values of specimens H-P1-T1U10 (A) and H-P2-T1U10 are greater than 100 mV. Hence the corrosion protection processes for the FRP retrofitted RC beams are effective. The ultimate strengths of beams H-P1-T1U10 (A) and H-P2-T1U10 are lower than the ultimate strength of beam H-O-T1U10, but are higher than the value of beam H-A1-ET1U10.

## Analytical Analysis

Research has shown that bond deterioration at the steel/concrete interface causes reinforcement corrosion, which reduces flexural strength (Mangat and Elgarf 1999). Saifullh and Clark (1994) have reported that the bond strength at the steel/concrete interface increased due to the confinement of the expansion of corrosion products during the early stages of the corrosion process. This radial stress confinement can be reduced for longer corrosion periods, to allow the corrosion products to dissipate gradually via the pore structure in the concrete matrix, or once expansion cracks have formed. In the present study we assumed that the stirrups would have a beneficial effect on the bonding strength of corroded reinforcement material in concrete due to the confinement they would provide. Moreover, injecting epoxy into major cracks formed by the expansion of the corrosion products should

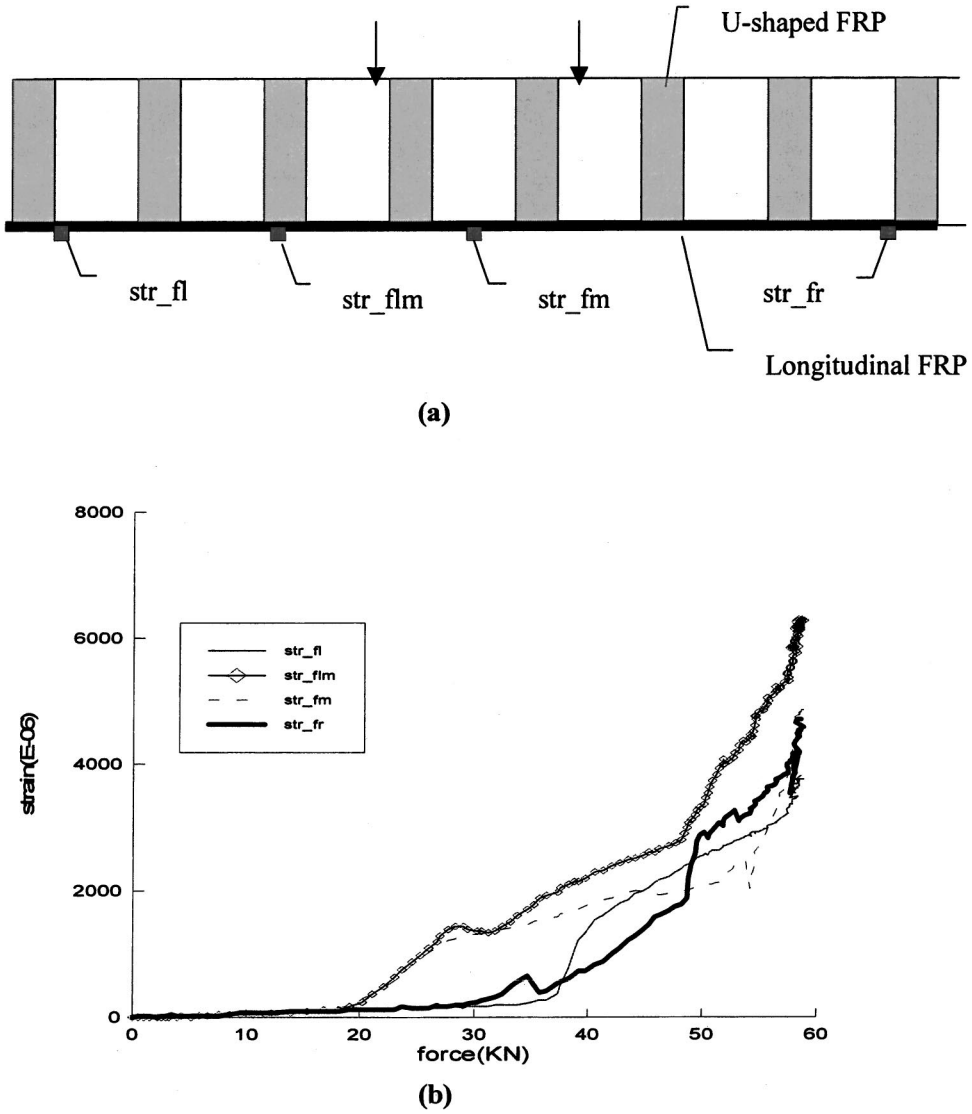


**Fig. 6.** Strain variations at some intersection points around the discontinuous U anchorage and longitudinal fiber-reinforced plastic strip on beam L-N-T1D10: (a) arrangement of strain gauges on the tensile side of the beam; and (b) strain data at various load levels

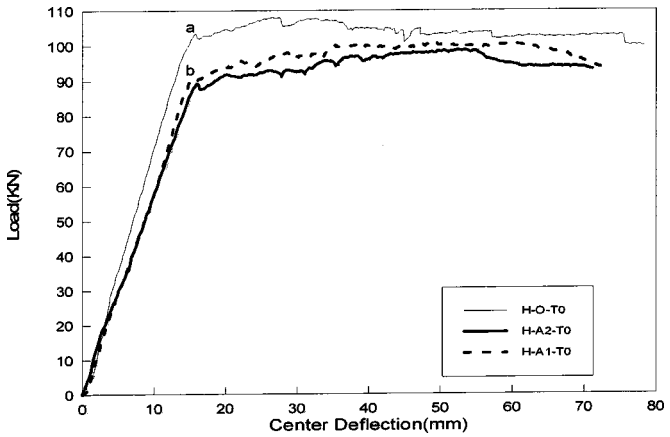


**Fig. 7.** Load-deflection curves of reinforced concrete beams for various corrosion states

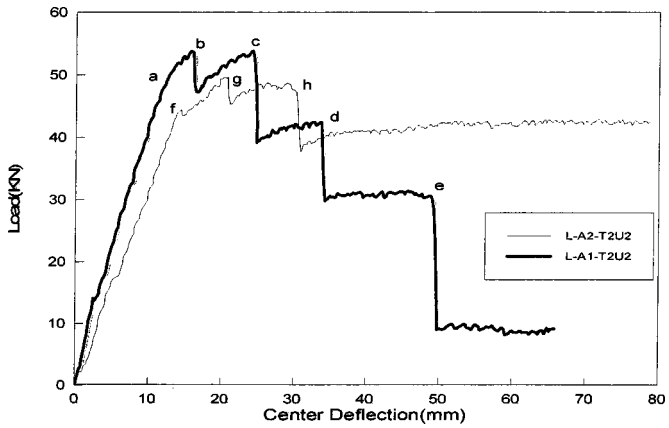


**Fig. 8.** Load deflection curves of reinforced concrete beams with and without pitting effects

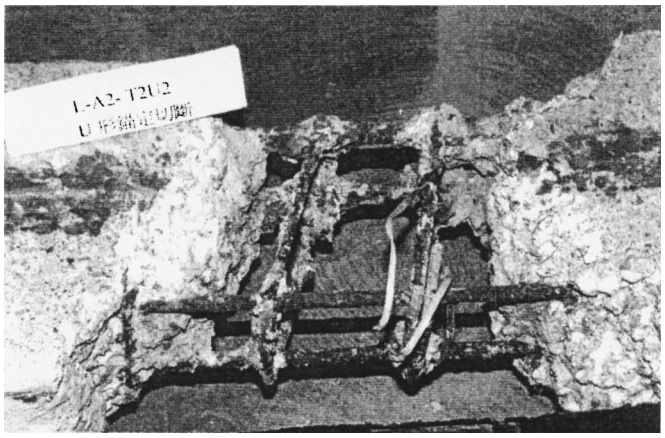


**Fig. 9.** Corrosion of reinforcement materials of beam L-A2-T2U2

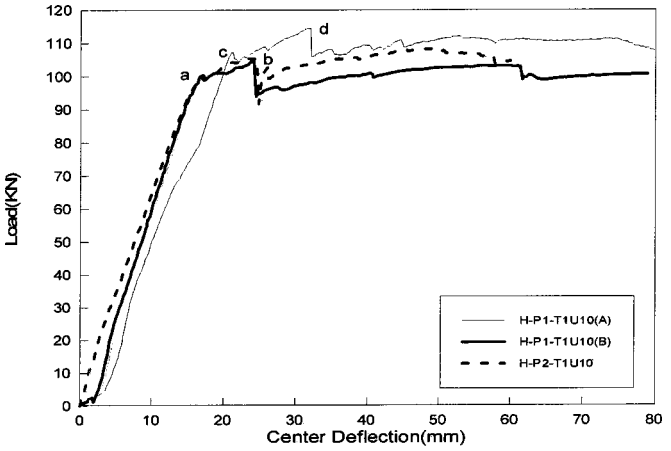


**Fig. 11.** Load-deflection responses of corrosion protected reinforced concrete beams: (a) H-P1-T1U10; (b) H-P1-T1U10; and (c) H-P2-T1U10

also provide some improvement of the bonding between the steel and the concrete. Therefore it is assumed that the prediction of the flexural strength by the standard composite mechanics expression, together with a suitable cross-sectional area of reinforcement for the resisting moment of beam, will be eligible. However, an extensive investigation on the effect of reinforcement corrosion on bonding in flexural elements still needs to be carried out by researchers.

To analyze the load-deflection response of the test beams, an analytical algorithm developed by Wang and Ling (1998) is used to predict the moment-curvature and load-deflection behavior of the FRP externally patched RC beams. The following basic assumptions are made: (1) planar sections remain planar after bending, (2) perfect bonding exists between the concrete and the reinforcement, and (3) the nonlinear stress-strain relationship for each material is known. With this strain compatibility method, the nonlinear moment-curvature relationship can be constructed through an iterative computation algorithm. Once the moment-curvature relationships for a beam's section are obtained, the deflection of the beam can then be determined by the moment-area method, according to the theories of the strength of material. Using this strain compatibility method and the nonlinear stress-strain relationships of steel and concrete, an anchorage shear failure model and a modified tooth peeling failure model were developed. This algorithm is capable of calculating the strain distribution, the internal forces across each cross section, and the interfacial shear stress distribution along the interface between the FRP strips and the concrete beams for different load levels. The onset and the propagation direction of the debonding process can be effectively analyzed.

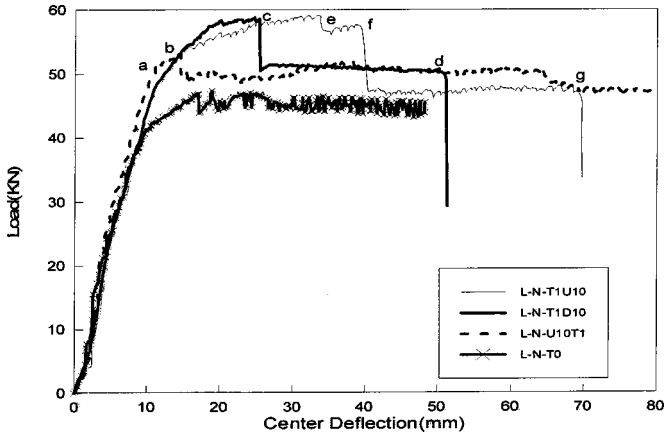


**Fig. 10.** Load-deflection responses for no corrosion, low compression strength concrete beams with various types of fiber-reinforced plastic strip arrangements

Another method of analyzing the ultimate flexural strength of FRP retrofitted RC beams has been proposed by Saadatmanesh and Malek (1998). This method provides guidelines and equations for the flexural strengthening of concrete beams using epoxy bonded fiber composite plates. It has to be pointed out that the diameter of the rebar used in the analytical analyses was reduced according to the corrosion damage state in Eqs. (2)–(4). The predicted ultimate strength values and the associated failure modes of all the beams tested by the Malek–Saadatmanesh method are also listed in Table 7.

Comparing the predicted ultimate strengths obtained by the two above-mentioned methods, one finds very small differences between most of the failure modes. The major difference is that the moment-curvature method can predict the entire load-deflection response and the load level when the longitudinal FRP strip debonding failure was initiated through the interfacial shear stress evaluation and the debonding failure criteria. It is seen in Table 7 that the moment-curvature method can predict the failure mode 4 (longitudinal FRP strips debonding) and match the experimental data quite well. However, Table 7 demonstrates that the current model's algorithm cannot predict the type (2) failure mode. The predicted ultimate loads for beams with a high value of compression strength are within 13% difference compared with the experimental results. In general, the predictions for the low compression strength group are not especially good for the beams suffering accelerated corrosion. This mismatching may be explained by the in-homogeneous distribution of the concrete material throughout the depth of the beam, which caused a shifting of the neutral axis of the resisting moment away from the prediction model. This analytical study demonstrates that a reduction in the steel reinforcement cross-sectional area due to corrosion is not the only thing that affects the load carrying capacity of corroded beams. The application of FRP patches can effectively overcome the reduction of the bonding strength between the corroded steel/concrete interface and improve the loading capacity of a corroded concrete beam.

## Conclusions

The behavior and potential of combining corrosion protection and FRP patching repair techniques to retrofit corrosion damaged RC beams is demonstrated. The equally spaced U-anchorage strips together with the longitudinal strips form an external reinforcing system for the corroded RC beam. This type of arrangement can improve the load carrying capacity of cracked and corroded RC beams and provides the space for coating the corrosion protection materials. However, the use of equally spaced U-anchorage strips to hold longitudinal strips constrains the extension of the fiber in the longitudinal direction in the intersection area. The strain value is higher at this site, but it enables the full usage of the fibrous composite material's strength. Hence any design that can reduce the stress concentration effect at the intersection area of the longitudinal and U-shaped anchorage strips may help the beam to escape from the premature failure mode of fiber breakage and reach its designed load carrying capacity. The analytical method proposed here by applying the rebar diameter reduction formula based on its corrosion rate can approximately predict the ultimate loads of FRP patched corroded beams. To establish a more rigorous prediction model, the bond strength reduction mechanism between the corroded steel/concrete interface must be considered. The confinement effect, from stirrups or externally patched FRP strips, may be an important factor to consider in this bond strength reduction model. This study demonstrates that a successful implementation of any new retrofitting strategy requires knowledge, not only of aspects related to the design, but also of the materials used and degradation and durability of joints and connections. This needs to be incorporated into the analysis of retrofitted structures to predict local effects on the entire structural system.

## Acknowledgment

The writers would like to acknowledge the National Science Council of Taiwan for the support of this research through contract number NSC-87-2211-E-008-023.

## Notation

*The following symbols are used in this paper:*

$A_i$ = total surface area of the number $i$ type rebar within reinforced concrete beam;
$D_i^C$ = diameter of number $i$ type rebar after accelerated corrosion;
$D_i^0$ = original diameter of number $i$ type rebar before corrosion testing;
$F$ = Faraday's constant (96,500 A s);
$f_c'$ = compression strength of concrete;
$I$ = current applied to the specimen;
$L_i$ = length of each rebar unit;
$M$ = atomic weight [$M$ (steel) = 56];
$N_i$ = total number of number $i$ type rebar units ($N_6 = 2$, $N_4 = 2$, $N_3 = 34$ in the present study);
$n$ = valence of the reacting electrode (iron) for the material ($n_{\text{steel}} = 2$);
$R$ = corrosion rate;
$S$ = total surface area of the reinforcement material within a specimen;
$t$ = time elapsed in hours after casting;
$\Delta V$ = total volume deduction of corrosive reinforcements in the specimen;
$\Delta V_i$ = volume deduction of number $i$ type rebar due to corrosion; and
$\rho$ = density of the material (7.8 g/cm$^3$ for steel).

## References

Dehwah, H. A. F., Basunbul, I. A., Maslehuddin, M., Al-Sulaimani, G. J., and Baluch, M. H. (1994). "Durability performance of repaired reinforced concrete beams." *ACI Mater. J.*, 91(2), 167–172.

Ehsani, M. R., and Saadatmanesh, H. (1990). "Fiber composite plates for strengthening bridge beams." *Compos. Struct.*, 15, 343–355.

GangaRao, H. V. S., and Vijay, P. V. (1998). "Bending behavior of concrete beams wrapped with carbon fabric." *J. Struct. Eng.*, 124(1), 3–10.

Jones, R. R., Swamy, R. N., Bloxham, J., and Bouderbalah, A. (1980). "Composite behavior of concrete beams with epoxy bonded external reinforcement." *Int. J. Cement Compos. Lightweight Concr.*, 292, 91–107.

Karbhari, V. M., and Engineer, M. (1996). "Effect of environmental explosure on the external strengthening of concrete with composites-short term bond durability." *J. Reinf. Plast. Compos.*, 15, 1194–1216.

Mangat, P. S., and Elgarf, M. S. (1999). "Flexural strength of concrete beams with corroding reinforcement." *ACI Struct. J.*, 96(1), 149–158.

Nanni, A., Focacci, F., and Cobb, C. A. (1998). "Proposed procedure for the design of RC flexural members strengthened with FRP sheets." *Fiber Composites in Infrastructure, Proc., 2nd Int. Conf. on Composites in Infrastructure*, Tucson, Ariz., H. Saadatmanesh and M. R. Ehsani, eds., Vol. I, 187–201.

Saadatmanesh, H., and Malek, A. M. (1998). "Design guidelines for flexural strengthening of RC beams with FRP plates." *J. Compos. Constr.*, 2(4), 158–164.

Saifullh, M., and Clark, L. A. (1994). "Effect of corrosion rate on the bond strength of corroded reinforcement," *Proc., Int. Conf. on Corrosion and Corrosion Protection of Steel and Concrete*, R. Narayan Swamy, ed., Sheffild Academic Press, 591–602.

Sonobe, Y., et al. (1997). "Design guidelines of FRP reinforced concrete building structures." *J. Compos. Constr.*, 1(3), 90–115.

Theriault, M., and Benmokrane, B. (1998). "Effects of FRP reinforcement ratio and concrete strength on flexural behavior of concrete beams." *J. Compos. Constr.*, 2(1), 7–16.

Wang, C. Y., and Ling, F. S. (1998). "Prediction model for the debonding failure of cracked RC beams with externally bonded FRP sheets." *Proc., 2nd Int. Conf. on Composite Structure, ICCI'98*, Tucson, Ariz., Vol. 1, 548–562.